AGU PUBLICATIONS

Geophysical Research Letters

RESEARCH LETTER

10.1002/2014GL062826

Key Points:
- First time smoke influence on tornado severity is shown for a real case study
- A new mechanism on how smoke can influence tornadoes is presented
- We show that aerosol effects should be considered in severe weather forecasts

Supporting Information:
- Text S1, Table S1, and Figures S1–S9

Correspondence to:
P. E. Saide and G. R. Carmichael,
pablo-saide@uiowa.edu;
gcarmich@engineering.uiowa.edu

Citation:
Saide, P. E., S. N. Spak, R. B. Pierce, J. A. Otkin, T. K. Schaack, A. K. Heidinger, A. M. da Silva, M. Kacenelenbogen, J. Redemann, and G. R. Carmichael (2015), Central American biomass burning smoke can increase tornado severity in the U.S., *Geophys. Res. Lett.*, *42*, doi:10.1002/2014GL062826.

Received 10 DEC 2014
Accepted 19 JAN 2015
Accepted article online 26 JAN 2015

Central American biomass burning smoke can increase tornado severity in the U.S.

P. E. Saide[1], S. N. Spak[1], R. B. Pierce[2], J. A. Otkin[3], T. K. Schaack[3], A. K. Heidinger[2], A. M. da Silva[4], M. Kacenelenbogen[5], J. Redemann[6], and G. R. Carmichael[1]

[1]Center for Global and Regional Environmental Research, University of Iowa, Iowa City, Iowa, USA, [2]NOAA Satellite and Information Service (NESDIS) Center for Satellite Applications and Research, Madison, Wisconsin, USA, [3]Cooperative Institute for Meteorological Satellite Studies, University of Wisconsin-Madison, Madison, Wisconsin, USA, [4]Global Modeling and data Assimilation Office, NASA Goddard Space Flight Center, Greenbelt, Maryland, USA, [5]BAER Institute/NASA Ames Research Center, Moffett Field, California, USA, [6]NASA Ames Research Center, Moffett Field, California, USA

Abstract Tornadoes in the Southeast and central U.S. are episodically accompanied by smoke from biomass burning in central America. Analysis of the 27 April 2011 historical tornado outbreak shows that adding smoke to an environment already conducive to severe thunderstorm development can increase the likelihood of significant tornado occurrence. Numerical experiments indicate that the presence of smoke during this event leads to optical thickening of shallow clouds while soot within the smoke enhances the capping inversion through radiation absorption. The smoke effects are consistent with measurements of clouds and radiation before and during the outbreak. These effects result in lower cloud bases and stronger low-level wind shear in the warm sector of the extratropical cyclone generating the outbreak, two indicators of higher probability of tornadogenesis and tornado intensity and longevity. These mechanisms may contribute to tornado modulation by aerosols, highlighting the need to consider aerosol feedbacks in numerical severe weather forecasting.

1. Introduction

Smoke from central American fires is transported episodically during spring to the southeastern (SE), central, and eastern United States (U.S.) [*Wang et al.*, 2009]. Observational evidence shows that given the preexisting conditions for supercell development, these smoke events can modulate severe weather outbreaks [*Lyons et al.*, 1998; *Murray et al.*, 2000]. Updraft invigoration through suppression of the onset of warm rain [*Andreae et al.*, 2004; *Koren et al.*, 2005] has been hypothesized as a mechanism by which smoke enhances severe weather [*Wang et al.*, 2009]. More generally, invigoration of deep convection by aerosols has been associated with increases in cloudiness [*Andreae et al.*, 2004], rain [*Bell et al.*, 2008], thunderstorm cloud heights [*Bell et al.*, 2009b], and lightning [*Yuan et al.*, 2011; *Bell et al.*, 2009a]. Microphysical processes have also been found to play an important role [*Fan et al.*, 2013]. Other observational [*Ackerman et al.*, 2000; *Li et al.*, 2011] and model [*Jiang and Feingold*, 2006; *Xue et al.*, 2008] evidence has indicated no effect, or even suppression, on cloudiness and convection as aerosol loads increase, which has been explained as a transition from invigoration to suppression [*Koren et al.*, 2008; *Rosenfeld et al.*, 2008; *Dagan et al.*, 2014]. Aerosol-cloud-radiation interactions remain an area of active research as they pose the greatest uncertainty in climate studies [*Boucher et al.*, 2013].

In spite of evidence highlighting aerosol impacts on atmospheric conditions, current numerical severe weather forecast models typically do not include aerosol interactions due to their observational and process-based uncertainties [*McFiggans et al.*, 2006] and generally high computational expense. In the case of tornadoes, studies have shown aerosol microphysical effects on tornadogenesis in idealized simulations [*Lerach et al.*, 2008; *Lerach and Cotton*, 2011]. *Rosenfeld and Bell* [2011] postulated that the weekly cycle of tornadoes can be modulated by weekday/weekend differences in anthropogenic aerosol sources, which has generated debate in terms of the methods used and the physical mechanisms proposed to explain aerosol effects on severe storms [*Yuter et al.*, 2013; *Rosenfeld and Bell*, 2013]. The influences of aerosols on the parameters commonly used in tornado forecasts have not been previously studied, and the effects of aerosols have not been resolved in historic cases.

In the following we analyze the effect of central American biomass burning on a historic severe weather outbreak that occurred during the afternoon and evening of 27 April 2011 [*Doswell et al.*, 2012]. This outbreak produced 122 tornadoes and resulted in 313 deaths across the southeastern U.S., with 68 tornadoes considered

©2015. American Geophysical Union. All Rights Reserved.

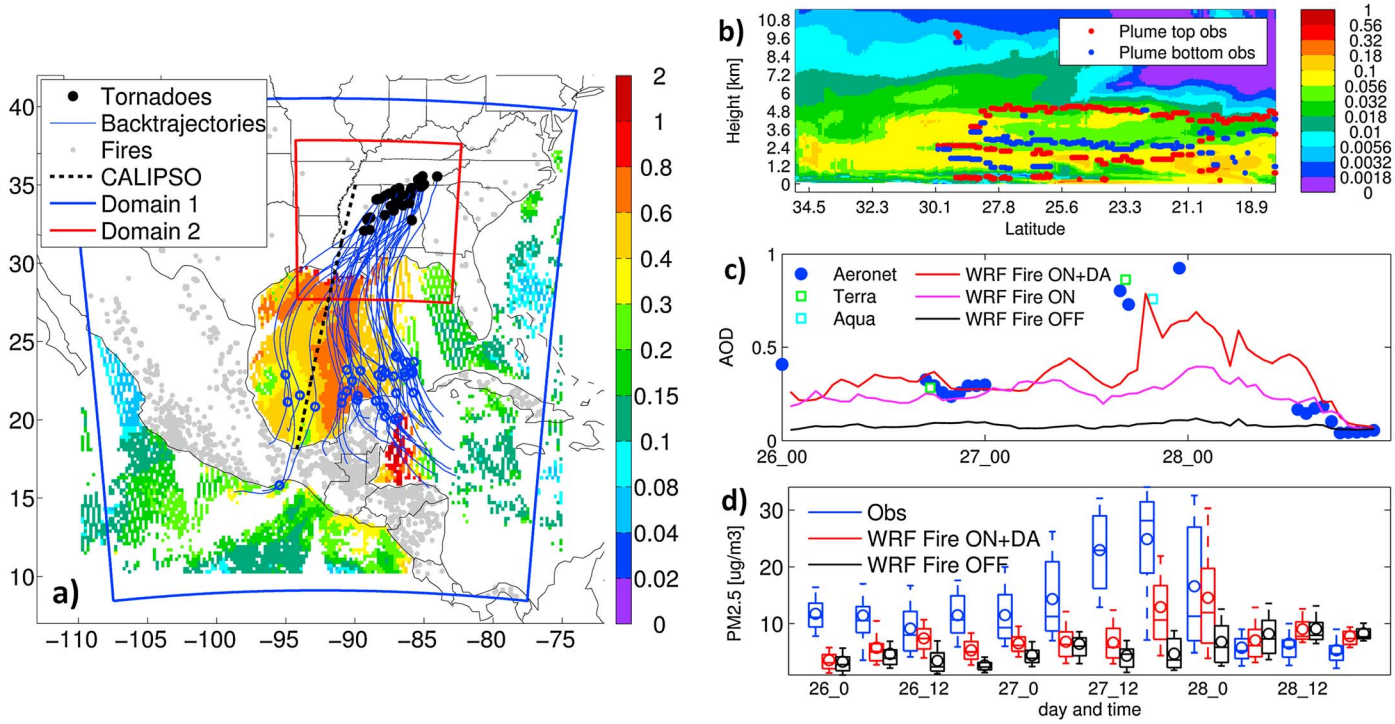

Figure 1. Biomass burning smoke before and during the outbreak of 27 April. (a) Back trajectories of 42 h performed with FLEXPART [*Fast and Easter*, 2006] from the beginning of violent tornado (EF4 and EF5) tracks, with circles marking 24 h, observed AOD over ocean on 27 April (contour color scale on the side), fire locations for the day before, CALIPSO track for 26 April at 8 UTC, and modeling domains. (b) Model aerosol extinction coefficient (1/km) profiles when including fire emissions overlaid by the smoke plumes top and bottom heights as measured by Cloud-Aerosol Lidar with Orthogonal Polarization for the CALIPSO track in Figure 1a. (c) Time series for modeled and observed AOD at the WaveCIS AERONET site (Figure S2). (d) Time series statistics as in Figure 2 every 6 h periods for all $PM_{2.5}$ coastal sites presented in Figure S2.

significant (EF2 or greater damage) and 15 considered violent (EF4 or EF5), and with the violent ones being responsible for almost 90% of the fatalities [*NOAA*, 2011]. The only outbreak ever recorded of a similar magnitude which also resulted in a similar number of mortalities occurred on 3 April 1974 [*Doswell et al.*, 2012]. By many metrics, 27 April 2011 is considered the most significant outbreak since 1950 [*Knupp et al.*, 2013]. The analysis of the outbreak is performed using models, observations, and data assimilation described in section 2. Section 3 investigates the smoke presence in the region of the outbreak and explores how the smoke can modify the parameters used to predict severe weather outbreaks and the mechanisms involved in this modification. We finally assess uncertainties in our approach and delineate future directions.

2. Methods

2.1. Modeling System

We used the chemistry version of the Weather Research and Forecasting (WRF-Chem) modeling system [*Grell et al.*, 2005] as a coupled aerosol, chemistry, and weather forecasting tool. The system was used to produce simulations using the CBM-Z (modified Carbon Bond Mechanism)-MOSAIC (Model for Simulating Aerosol Interactions and Chemistry) chemistry and aerosol treatment [*Zaveri and Peters*, 1999; *Zaveri et al.*, 2008] which can model aerosol effects on radiation and on cloud microphysics [*Fast et al.*, 2006; *Chapman et al.*, 2009], the latter by using a critical supersaturation activation scheme [*Abdul-Razzak and Ghan*, 2002] and two-moment bulk microphysics [*Morrison et al.*, 2009]. This allows assessing the impacts of smoke by turning on (Fire ON) and off (Fire OFF) biomass burning emissions, which were obtained from the Quick Fire Emission Dataset [*Darmenov and da Silva*, 2014]. An additional simulation (no Abs) was performed to assess the role of soot absorption by removing it (imaginary part of the soot refractive index set to 0). WRF-Chem was configured using a 12 km horizontal grid spacing outer domain including the smoke source region (Figure 1a), and a nested 4 km domain was used to resolve convection (as done by NOAA predictions of severe storms and hurricanes) and for the incorporation of aerosol indirect effects. The model had 52 vertical levels: the first five levels had ~50 m

©2015. American Geophysical Union. All Rights Reserved.

thickness; there were 11 and 19 levels within the lowermost 1 km and 3 km layers, respectively; and the uppermost levels had ~400 m thickness and reached a top pressure of 50 hPa (~18 km). The outer domain simulations spanned from 17 to 29 April 2011. This spin-up period allowed time for simulations with and without fire emissions to differentiate in terms of its smoke loads and response to aerosol feedbacks. The inner domain was driven through one-way nesting starting at 00 UTC on 26 April. Additional details of the WRF-Chem configuration can be found in the supporting information Text S1, section 1.1.

2.2. Data Assimilation

Biomass burning emission estimates are generally highly uncertain, which can produce large errors in smoke concentrations [*Kaiser et al*., 2012]. In order to increase the accuracy of smoke simulations and thus assess the impacts of smoke loadings closer to those observed, additional simulations were performed introducing satellite aerosol optical depth (AOD) data assimilation (Fire ON + DA) using the Grid-point Statistical Interpolation system [*Kleist et al*., 2009; *Saide et al*., 2013]. Biomass burning was the predominant source of aerosol for the period analyzed in central American and the Gulf of Mexico (GoM) (section 3.1); thus, assimilation of AOD mainly scales smoke concentrations, and it is reasonable to assign the effects of additional aerosol generated by the assimilation of smoke particles. Assimilation was performed every 3 h throughout the simulation, starting from 20 April on the coarse domain and from 26 April on the inner domain, respectively, and each assimilation step was followed by a 3 h WRF-Chem forecast which was restarted from the previous cycle and where only aerosol initial conditions were modified. An additional simulation was performed with no soot absorption (Fire ON + DA, no Abs) as described in section 2.1. Additional details on the assimilation configuration can be found in the supporting information Text S1, section 1.1.

2.3. Tornado Parameters

Operational prediction centers use regional-scale models to forecast the meteorological conditions (tornado parameters) that increase the likelihood of tornado occurrence and severity [*Thompson et al*., 2003; *Rasmussen and Blanchard*, 1998]. We computed these parameters for each simulation and used them to assess the smoke impacts. The Unified Post Processor v2.0 [(Developmental Testbed Center: Unified Post Processor, 2012, http://www.dtcenter.org/wrf-nmm/users/overview/upp_updates.php)] was used to compute lifting condensation level height (LCL), convective available potential energy based on the lowest 100 hPa mean parcel (CAPE), wind shear (0–1 and 0–6 km), and 0–1 km storm relative helicity (SRH), the latter computed with the dynamic method [*Bunkers et al*., 2000]. The significant tornado parameter (STP) was then computed from these variables [*Thompson et al*., 2003]:

$$\mathrm{STP} = \left(\frac{\mathrm{CAPE}[\mathrm{J/kg}]}{1000[\mathrm{J/kg}]}\right)\left(\frac{0-6\ \mathrm{km\ shear}[\mathrm{m/s}]}{20[\mathrm{m/s}]}\right)\left(\frac{\mathrm{SRH}[\mathrm{m^2/s^2}]}{100[\mathrm{m^2/s^2}]}\right)\left(\frac{2000[\mathrm{m}]-\mathrm{LCL}[\mathrm{m}]}{1500[\mathrm{m}]}\right) \quad (1)$$

An intensification of these parameters was defined as changes leading to a stronger outbreak, which corresponds to a reduction in LCL and an increase in all other parameters.

2.4. Observations

Several meteorological and atmospheric composition measurements were used to assess model performance, smoke presence, and its impacts. These included satellite observations of 550 nm AOD by the NASA Neural Network Retrieval, which improved model performance when included in data assimilation systems [*Saide et al*., 2013]: ground-based measurements of aerosol optical properties by Aerosol Robotic Network (AERONET), plume heights retrieved by the CALIPSO, satellite cloud optical depth (COD) retrieved by Moderate Resolution Imaging Spectroradiometer (MODIS), and downward shortwave radiation from the U.S. Regional Climate Reference Network (USRCRN). Details of these and other supporting observations are described in Table S1, and locations of the ground sites are illustrated in Figure S2.

2.5. Statistical Analysis

In the case of tornado parameters (e.g., Figure 2), mean "near-storm environments" within a 185 km radius [*Thompson et al*., 2012] from each tornado starting point were used to build statistics and statistical significance was assessed using a paired two-tailed *t* test at the 5% *p* value level. Tornadoes included in the statistics were those with tornadogenesis occurring in the "Tornado region." This region contained the most significant tornadoes and included the area where the model showed convective cells with supercell characteristics (Text S1, section 2.1) and where shallow clouds were properly represented (Text S1, section 2.2). For variables

©2015. American Geophysical Union. All Rights Reserved.

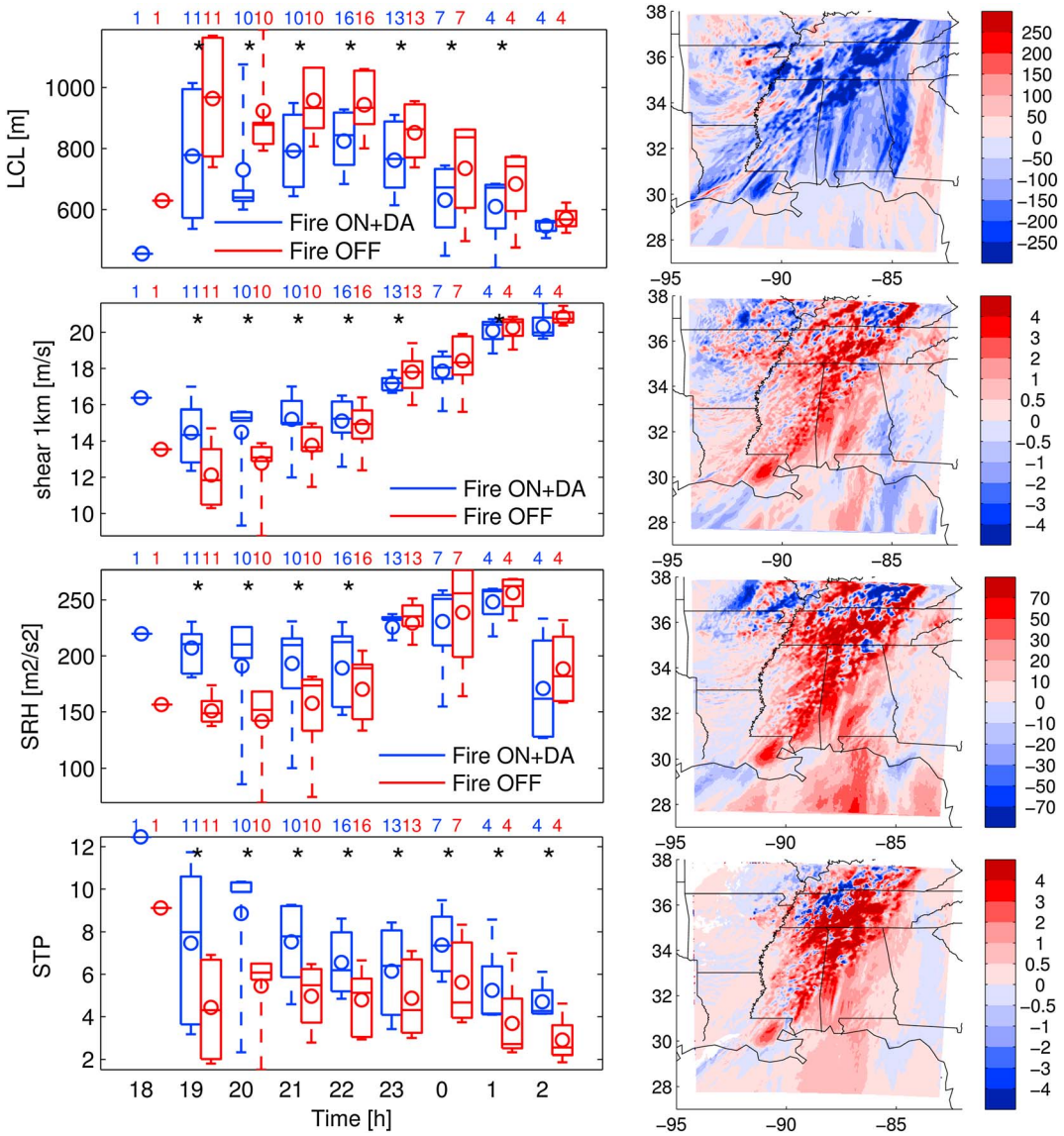

Figure 2. (left) Statistics of parameters used in tornado forecasting from simulations Fire ON + DA and Fire OFF. Statistics are computed for the mean near-storm environment for each tornado starting over portions of Mississippi, Alabama, Tennessee, and Georgia (see Tornado region in Figure S2) with numbers on top of each panel representing the number of tornadoes that go into the statistics and "asterisk" indicating significant differences at the 5% *p* value level. Boxes represent the 25th and 75th percentiles, whiskers show the 10th and 90th percentiles, and mean and median are indicated with a circle and horizontal line, respectively. (right) Maps of mean differences from 18 to 00 UTC between Fire ON + DA and Fire OFF.

other than tornado parameters (cloud optical depth, radiation, and others in the supporting information), statistics were computed for model grid cells contained in a given region (Tornado region and "inflow region"), and a two-sample two-tailed *t* test was used to assess statistical significance at the 5% *p* value level. The inflow region (Figure 3) covered the warm sector of the extratropical cyclone approximately 3 h before the outbreak and was used to analyze the inflow conditions to the Tornado region.

3. Results

3.1. Smoke Presence During the Outbreak

Simulations and observations indicate that smoke from central American biomass burning was present in the boundary layer and lower free troposphere before and during the storm outbreak. Smoke was found over the GoM as supported by the high and extensive MODIS AOD (Figure 1a), the significant number of fire

©2015. American Geophysical Union. All Rights Reserved.

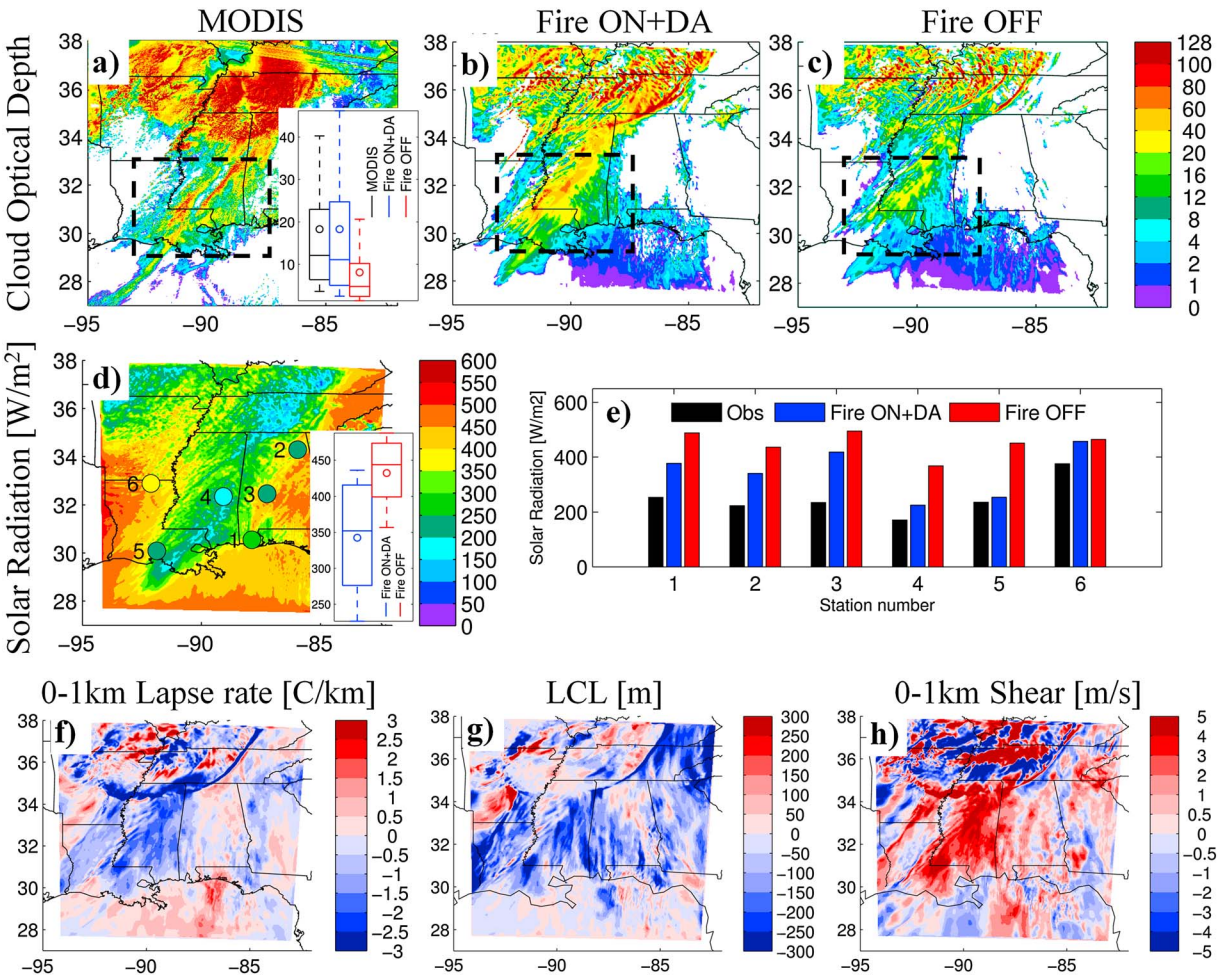

Figure 3. (a) MODIS COD from Terra overpass at 16:30 UTC on 27 April (~3 h before the outbreak starts) and simulation estimates (b) with fire emissions and data assimilation and (c) without fire emissions. An insert in Figure 3a illustrates observed and modeled statistics as in Figure 2 over the inflow region (segmented line rectangle). Fire ON + DA and MODIS COD distributions are not significantly different while Fire OFF and MODIS distributions are different at the 5% significance level. (d) Average solar radiation for the model with fire emissions and data assimilation with color-coded circles representing USRCRN average observations for 27 April daytime, with an insert showing model statistics over the inflow region. Fire ON + DA and Fire OFF radiation distributions are significantly different at the 5% level. (e) Observed and modeled solar radiation for stations in Figure 3d. (f–h) Difference between model variables for the Fire ON + DA and Fire OFF simulations at 16 UTC.

detections south and west of the GoM (Figure 1a), the substantially better model representation of aerosol observations when smoke emissions were included (Fire ON, Figures 1c and S1), and the lack of other sources (such as dust) coming from the boundaries (Figures 1a and S1). Fires were the main source of aerosols in the inflow region of the storm as back trajectories come from the polluted area of the Gulf (Figure 1a), the area which also provided the warm and moist air necessary for the outbreak to occur [*Knupp et al.*, 2013]. Also, the model represented the three aerosol vertical layers over the GoM below 5 km on 26 April, which were heavily influenced by smoke (Figure 1b). The modeled aerosol layer at 5–8 km altitude and north of 25°N not represented by the observations was not of smoke origin (it was also found in the Fire OFF simulation, not shown) and was likely not resolved by CALIPSO due to its lower concentrations. Although the Fire ON simulation captured the smoke, it underestimated its loads, largely due to underestimates in the emissions. Data assimilation substantially improved model representation of increase in AOD due to smoke at the southern Louisiana AERONET site (Figure 1c) but underestimated the $PM_{2.5}$ increase (Figure 1d), possibly due to clouds blocking satellite AOD retrievals. However, the Fire ON + DA $PM_{2.5}$ predictions achieved the performance goal (the best that a model can be expected to achieve) and criteria (level of accuracy accepted for air quality applications) air quality metrics [*Boylan and Russell*, 2006] 38% and 93% of the time during this event, respectively. The Angstrom exponent (AE), an indicator of the aerosol size distribution [*Schuster et al.*, 2006], was well represented only by simulations including fire emissions, as mean observed 440–870 nm AE at the AERONET site

©2015. American Geophysical Union. All Rights Reserved.

on 27 April was 1.2, while it reached 1.0 and 0.2 for simulations Fire ON + DA and Fire OFF, respectively. In the Fire OFF case the low AE was due to coarse sea-salt particles from the GoM. The size distribution was shifted toward finer particles due to the smoke presence. AE was slightly underestimated in the Fire ON + DA case, likely due to uncertainties in the prescribed size distribution of the smoke assumed in the emissions. By the end of 28 April the smoke no longer influenced the SE U.S. and all simulations had similar AOD values and were in agreement with the observations (Figure 1c). Evidence of smoke over the GoM and over the continent as depicted here is not uncommon and has also been detected in other severe weather events [*Wang et al.*, 2009].

3.2. Impacts on Tornado Parameters

Simulations permitting aerosol interactions showed that within an environment already conducive to severe thunderstorm development, biomass burning smoke intensified the LCL, low-level (0–1 km layer) wind shear, and SRH in close proximity to the tornado locations (Figure 2). In particular, the influence of smoke generated statistically significant lower LCL (100–200 m lower before 28 April 00 UTC) and higher SRH (up to ~50 m^2/s^2 hourly mean) and wind shear (up to ~2 m/s hourly mean) in the vicinity of the earlier tornadoes from the afternoon outbreak, which were the most numerous and intense tornadoes. STP also increased (1.3 to 3.4 higher in hourly mean before 28 April 00 UTC) due to the intensification of LCL and SRH (equation (1)), as CAPE and 0–6 km shear differed by less than 7% and 3%, respectively, between simulations for the same period (Text S1, section 2.3). LCL, low-level shear, SRH, and STP are important parameters in discriminating between supercell classes (significant tornadic, weak-tornadic, and nontornadic) and tornado categories [*Thompson et al.*, 2003; *Markowski et al.*, 2002, 2003; *Markowski and Richardson*, 2009; *Thompson et al.*, 2012]. Although simulations with and without smoke both predicted values necessary for supercell and tornado development [*Thompson et al.*, 2003], and were consistent with the analysis values [*Knupp et al.*, 2013], the differences in tornado parameters between these simulations may have substantial impact on tornado occurrence and intensity as they were of similar magnitude as the mean differences found in the sounding climatology within adjacent supercell classes [*Thompson et al.*, 2003, 2012]. These effects were not an artifact of assimilating AOD, as similar results were found for the Fire ON simulation (Figure S3a). Also, similar smoke effects were obtained when decreasing model resolution and when configuring the model with different microphysics and boundary layer schemes (Figures S3b–S3d), demonstrating the robustness of these impacts. Thus, these results suggest that the presence of biomass burning smoke can promote the development of conditions under which violent tornadoes, like those observed during the outbreak of April 27 and responsible for most of the fatalities, are more likely to happen. Accumulated rainfall and cloud top height statistics were also influenced by smoke (Text S1, sections 2.1 and 2.2), resulting in changes in the location of convective cells and precipitation patterns. However, smoke effects generated slightly lower rain rates (both in mean and upper ends of the distribution) and lower cloud top heights, thereby providing no evidence that invigoration occurred for these simulated storms. Instead, these results point toward a slight reduction in convective vigor by smoke radiative effects during this event, consistent with prior studies such as *Koren et al.* [2008] and *Rosenfeld et al.* [2008].

3.3. Mechanism

Mesoscale meteorological analysis was used to identify the driving mechanisms for the intensification of various tornado parameters in the absence of modeled convection invigoration. At the beginning of the outbreak (18 UTC), shallow multilayer stratiform clouds (top heights < 3 km) were observed and modeled across the region (Figures 3a–3c), which persisted throughout the day (Figure S4). The presence of smoke increased the simulated cloud condensation nuclei concentrations (increased aerosol number dominated over decrease in bulk hygroscopicity), which increased the number of cloud droplets, decreased drizzle rates, and increased liquid water content through the first and second aerosol indirect effects [*Twomey*, 1991; *Albrecht*, 1989]. As a result, stratiform clouds in the warm sector of the extratropical cyclone became optically thicker (Figures 3a–3c), which reduced the amount of solar radiation reaching the ground (Figures 3d and 3e), suppressed heat fluxes from the surface, and produced lower surface temperatures and a more stable boundary layer, shown by the reduction in the low-level lapse rate (Figure 3f). These conditions reduced mixing close to the surface and led to lower LCL (Figure 3g) through a shallower boundary layer and stronger low-level shear (Figure 3h) through increased vertical gradients. SRH also increased as it is intimately related to wind vertical gradients [e.g., *Markowski et al.*, 2003]. Along with increased stability, lower cloud bases were obtained due to thicker cloud layers (for clouds capping the boundary layer) and reduced surface temperature (the air reaches saturation more quickly during lifting).

©2015. American Geophysical Union. All Rights Reserved.

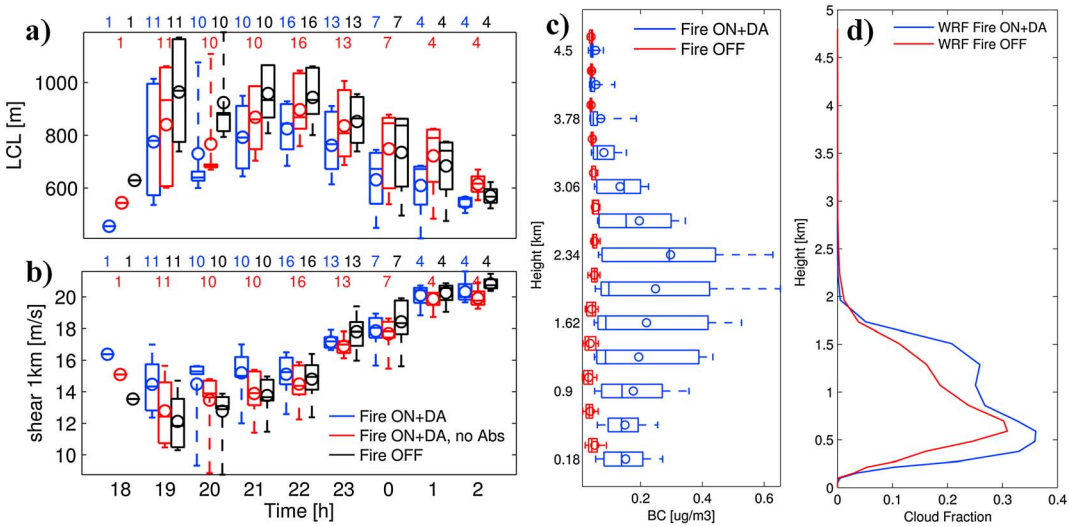

Figure 4. (a, b) Hourly box and whisker distributions as in Figure 2 for simulations with fire emissions and data assimilation (Fire ON + DA), fire emissions and data assimilation with black carbon absorption set to 0 (Fire ON + DA, no Abs), and no fire emissions (Fire OFF). (c, d) Statistics for vertical profiles at 16 UTC over the inflow region (Figure 3) for simulations Fire ON + DA and Fire OFF. Box and whisker plots are shown for soot concentrations (BC, Figure 4c) while solid lines represent mean cloud fraction (Figure 4d).

Observed COD was better represented by the model when smoke was included in the simulations for both a MODIS overpass (Figures 3a–3c) and for geostationary data throughout the day (Figure S4). The same was true for surface downwelling shortwave radiation. While the simulations missed some observed clouds (eastern part of the box in Figures 3a–3c) producing an overestimation of solar radiation in stations 1–3 and a slight performance improvement by the smoke presence (Figure 3e), the bias was considerably lower when smoke was present for stations 4 and 5 (55 and 18 W/m^2 bias, respectively, for the Fire ON + DA simulation) where a better cloud representation was found. Thus, observed shallow cloud properties and atmospheric conditions were consistent with the impacts of smoke illustrated by the model. The smoke effects were more significant for the earlier tornadoes during the afternoon outbreak (18–23 UTC, Figure 2), as the mechanism is driven by solar radiation, and these effects dissipated after sunset.

Soot (black carbon), responsible for 1–4% of the biomass burning smoke mass emitted in the simulation, was found to play an important role in cloud dynamics (Figures 4a and 4b). Sensitivity simulations with no soot absorption (but same smoke mass loading) indicated that it contributed on average 40%, 57%, and 81% of the enhancements in LCL, low-level shear, and SRH, respectively, for tornadoes occurring between 18 and 00 UTC. Black carbon over the region feeding the outbreak was found predominantly above clouds (Figures 4c and 4d). Previous research has found that absorption of radiation by elevated smoke plumes stabilizes the atmosphere below and can generate changes in clouds, with general enhancements over oceanic stratocumulus and reductions over land [*Koch and Del Genio*, 2010]. In this study, in addition to cloud thickening by indirect radiative effects described above, soot absorption heated the aerosol layer aloft (Text S1, section 2.3), stabilized the lower troposphere, and strengthened the capping inversion. This reduced entrainment of dry air resulted in a moister boundary layer and enhanced cloud cover below the aerosol layer. These effects were similar to the ones for smoke above stratocumulus clouds [*Brioude et al.*, 2009; *Wilcox*, 2010] and differed from effects that typically occur over land, as there was no moisture restriction due to the transport from the GoM [*Knupp et al.*, 2013]. These conditions resulted in lower cloud bases and stronger low-level wind shear, thereby leading to a higher probability of violent tornadoes in the simulations including smoke (see Text S1, section 2.3). Under the conditions of the outbreak, the impacts intensified as soot absorption above and between clouds was enhanced by the presence of multiple layers of optically thick clouds, which reflected light back to the soot layer more efficiently, and produced more absorption [*Haywood and Ramaswamy*, 1998; *Chung and Seinfeld*, 2005].

©2015. American Geophysical Union. All Rights Reserved.

4. Discussion

The presence of smoke generates a slight decrease in the model convective vigor (lower convective cloud top heights and rain rates) but at the same time leads to a lower cloud base within the region of tornado development, which has been associated with higher buoyancy in the rear flank downdraft leading to more likely tornadogenesis and increased tornado intensity and longevity [*Markowski et al*., 2002]. Furthermore, reduced vertical mixing can increase the low-level shear, which together with the LCL can be used to discriminate between nontornadic and tornadic supercells [*Markowski and Richardson*, 2009]. Thus, we hypothesize that the lower LCL and increased low-level shear overcome the decrease in convective vigor, thereby resulting in a net increase in tornado likelihood and severity. Storm-resolving large eddy simulations (LES) that are better able to depict tornadic circulations will be performed in future studies to test these hypotheses and further understand the impacts of smoke on near-storm environments and tornado occurrence, intensity, and longevity. LES models will also help test hypotheses such as if increased low-level stability due to the smoke presence can promote stronger storms, as previous studies have suggested that isolated, long-lived supercells can form when they move into an inversion region where secondary storms are suppressed [*Ziegler et al*., 2010].

These results show that for the case considered, the likelihood of significant tornado occurrence increased when smoke was present and that this was due to stabilization by soot and an increase in optical thickness in lower tropospheric clouds. Similar effects could potentially be generated by anthropogenic aerosols, as it has been found that they can increase optical depths of continental shallow clouds [*Berg et al*., 2011; *Rosenfeld*, 2000]. Furthermore, the enhanced low-level shear due to the combination of aerosol absorption and indirect radiative effects likely impact other mesoscale phenomena, including nontornadic severe weather events (e.g., thunderstorms, hail, and damaging straight-line winds).

The National Weather Service vision for 2020 is to move toward a "warn-on-forecast" paradigm for hazardous convective weather [*Stensrud et al*., 2009]. A warn-on-forecast system would rely on high-resolution ensemble predictions, using convection-resolving models with explicit microphysics and radar data assimilation to provide probabilistic convective-scale analyses and forecasts. Our findings, along with recent studies of tropical cyclones [*Dunstone et al*., 2013; *Rosenfeld et al*., 2011; *Evan et al*., 2011], highlight that aerosols can play an important role in modifying severe weather conditions. The inclusion of these aerosol feedbacks in weather forecasting models, as has been advocated by the scientific community [*Grell and Baklanov*, 2011] and recently implemented in some operational centers [e.g., *Morcrette et al*., 2009; *Mulcahy et al*., 2014], is expected to help improve the predictability of these extreme events. However, further work is needed to investigate effects of smoke on other tornado outbreaks and to assess the representation of these effects by computationally cost efficient aerosol models, which are feasible to use in operational weather forecasts [e.g., *Thompson and Eidhammer*, 2014], without decreasing predictive skill. We expect these processes to improve the timeliness and accuracy of severe weather alerts within future operational forecast systems.

Acknowledgments
We thank Robert Rabin, Jack Kain, and multiple anonymous reviewers for their comments that helped improve the study. We also thank Bill Gibson, Alan Weidemann, and their staff for establishing and maintaining the WaveCIS AERONET site used in this investigation. CALIPSO and MODIS data were obtained from the NASA Langley Research Center Atmospheric Science Data Center. This work was carried out with the aid of NASA grants NNX08AL05G and NNX11AI52G, EPA grant 83503701, grant UL1RR024979 from the National Center for Research Resources (NCRR), a part of the National Institutes of Health (NIH), and Fulbright-CONICYT scholarship 15093810. J.A.O. was supported by NOAA CIMSS grant NA10NES4400013 under the GOES-R Risk Reduction and GOES-R Algorithm Working Group programs. The views, opinions, and findings contained in this report are those of the author(s) and should not be construed as an official National Oceanic and Atmospheric Administration, U.S. Government, and other funding institutions position, policy, or decision. Contact P.E. Saide (pablo-saide@uiowa.edu) or G.R. Carmichael (gregory-carmichael@uiowa.edu) for data and code requests.

The Editor thanks two anonymous reviewers for their assistance in evaluating this paper.

References

Abdul-Razzak, H., and S. J. Ghan (2002), A parameterization of aerosol activation: 3. Sectional representation, *J. Geophys. Res.*, *107*(D3), 4026, doi:10.1029/2001JD000483.

Ackerman, A. S., O. Toon, D. Stevens, A. Heymsfield, V. Ramanathan, and E. Welton (2000), Reduction of tropical cloudiness by soot, *Science*, *288*, 1042.

Albrecht, B. A. (1989), Aerosols, cloud microphysics, and fractional cloudiness, *Science*, *245*, 1227.

Andreae, M. O., D. Rosenfeld, P. Artaxo, A. A. Costa, G. P. Frank, K. M. Longo, and M. A. F. Silva-Dias (2004), Smoking rain clouds over the Amazon, *Science*, *303*, 1337–1342, doi:10.1126/science.1092779.

Bell, T. L., D. Rosenfeld, K.-M. Kim, J.-M. Yoo, M.-I. Lee, and M. Hahnenberger (2008), Midweek increase in U.S. summer rain and storm heights suggests air pollution invigorates rainstorms, *J. Geophys. Res.*, *113*, D02209, doi:10.1029/2007JD008623.

Bell, T. L., D. Rosenfeld, and K.-M. Kim (2009a), Weekly cycle of lightning: Evidence of storm invigoration by pollution, *Geophys. Res. Lett.*, *36*, L23805, doi:10.1029/2009GL040915.

Bell, T. L., J.-M. Yoo, and M.-I. Lee (2009b), Note on the weekly cycle of storm heights over the southeast United States, *J. Geophys. Res.*, *114*, D15201, doi:10.1029/2009JD012041.

Berg, L. K., C. M. Berkowitz, J. C. Barnard, G. Senum, and S. R. Springston (2011), Observations of the first aerosol indirect effect in shallow cumuli, *Geophys. Res. Lett.*, *38*, L03809, doi:10.1029/2010GL046047.

Boucher, O., et al. (2013), Clouds and aerosols, in *Climate Change 2013: The Physical Science Basis. Contribution of Working Group I to the Fifth Assessment Report of the Intergovernmental 25 Panel on Climate Change*, edited by T. F. Stocker et al., Cambridge Univ. Press, Cambridge, U. K., and New York.

Boylan, J. W., and A. G. Russell (2006), PM and light extinction model performance metrics, goals, and criteria for three-dimensional air quality models, *Atmos. Environ.*, *40*, 4946–4959, doi:10.1016/j.atmosenv.2005.09.087.

©2015. American Geophysical Union. All Rights Reserved.

Brioude, J., et al. (2009), Effect of biomass burning on marine stratocumulus clouds off the California coast, *Atmos. Chem. Phys.*, *9*, 8841–8856, doi:10.5194/acp-9-8841-2009.

Bunkers, M. J., B. A. Klimowski, J. W. Zeitler, R. L. Thompson, and M. L. Weisman (2000), Predicting supercell motion using a new hodograph technique, *Weather Forecasting*, *15*, 61–79, doi:10.1175/1520-0434(2000)015<0061:psmuan>2.0.co;2.

Chapman, E., W. Gustafson Jr., R. Easter, J. Barnard, S. Ghan, M. Pekour, and J. Fast (2009), Coupling aerosol-cloud-radiative processes in the WRF-Chem model: Investigating the radiative impact of elevated point sources, *Atmos. Chem. Phys.*, *9*, 945–964.

Chung, S. H., and J. H. Seinfeld (2005), Climate response of direct radiative forcing of anthropogenic black carbon, *J. Geophys. Res.*, *110*, D11102, doi:10.1029/2004JD005441.

Dagan, G., I. Koren, and O. Altaratz (2014), Competition between core and periphery-based processes in warm convective clouds—From invigoration to suppression, *Atmos. Chem. Phys. Discuss.*, *14*, 23,555–23,581, doi:10.5194/acpd-14-23555-2014.

Darmenov, A., and A. M. da Silva (2014), The Quick Fire Emissions Dataset (QFED)—Documentation of versions 2.1, 2.2 and 2.4, NASA TM-2013-104606, vol. 35, 183 pp. [Available at http://gmao.gsfc.nasa.gov/pubs/tm/.]

Doswell, C. A., III, G. W. Carbin, and H. E. Brooks (2012), The tornadoes of spring 2011 in the USA: An historical perspective, *Weather*, *67*, 88–94, doi:10.1002/wea.1902.

Dunstone, N. J., D. M. Smith, B. B. B. Booth, L. Hermanson, and R. Eade (2013), Anthropogenic aerosol forcing of Atlantic tropical storms, Nature Geosci, advance online publication, doi:10.1038/ngeo1854. [Available at http://www.nature.com/ngeo/journal/vaop/ncurrent/abs/ngeo1854.html#supplementary-information.]

Evan, A. T., J. P. Kossin, C. '. E.'. Chung, and V. Ramanathan (2011), Arabian Sea tropical cyclones intensified by emissions of black carbon and other aerosols, *Nature*, *479*, 94–97. [Available at http://www.nature.com/nature/journal/v479/n7371/abs/nature10552.html#supplementary-information]

Fan, J., L. R. Leung, D. Rosenfeld, Q. Chen, Z. Li, J. Zhang, and H. Yan (2013), Microphysical effects determine macrophysical response for aerosol impacts on deep convective clouds, *Proc. Natl. Acad. Sci. U.S.A.*, *110*, E4581–E4590, doi:10.1073/pnas.1316830110.

Fast, J. D., and R. C. Easter (2006), A Lagrangian particle dispersion model compatible with WRF, 7th Annual WRF User's Workshop, 19–22.

Fast, J. D., W. I. Gustafson Jr., R. C. Easter, R. A. Zaveri, J. C. Barnard, E. G. Chapman, G. A. Grell, and S. E. Peckham (2006), Evolution of ozone, particulates, and aerosol direct radiative forcing in the vicinity of Houston using a fully coupled meteorology-chemistry-aerosol model, *J. Geophys. Res.*, *111*, D21305, doi:10.1029/2005JD006721.

Grell, G., and A. Baklanov (2011), Integrated modeling for forecasting weather and air quality: A call for fully coupled approaches, *Atmos. Environ.*, *45*, 6845–6851, doi:10.1016/j.atmosenv.2011.01.017.

Grell, G., S. E. Peckham, R. Schmitz, S. A. McKeen, G. Frost, W. C. Skamarock, and B. Eder (2005), Fully coupled "online" chemistry within the WRF model, *Atmos. Environ.*, *39*, 6957–6975, doi:10.1016/j.atmosenv.2005.04.027.

Haywood, J. M., and V. Ramaswamy (1998), Global sensitivity studies of the direct radiative forcing due to anthropogenic sulfate and black carbon aerosols, *J. Geophys. Res.*, *103*, 6043–6058, doi:10.1029/97JD03426.

Jiang, H., and G. Feingold (2006), Effect of aerosol on warm convective clouds: Aerosol-cloud-surface flux feedbacks in a new coupled large eddy model, *J. Geophys. Res.*, *111*, D01202, doi: 10.1029/2005JD006138.

Kaiser, J. W., et al. (2012), Biomass burning emissions estimated with a global fire assimilation system based on observed fire radiative power, *Biogeosciences*, *9*, 527–554, doi:10.5194/bg-9-527-2012.

Kleist, D. T., D. F. Parrish, J. C. Derber, R. Treadon, W.-S. Wu, and S. Lord (2009), Introduction of the GSI into the NCEP global data assimilation system, *Weather Forecasting*, *24*, 1691–1705.

Knupp, K. R., et al. (2013), Meteorological overview of the devastating 27 April 2011 tornado outbreak, *Bull. Am. Meteorol. Soc.*, *95*, 1041–1062, doi:10.1175/bams-d-11-00229.1.

Koch, D., and A. D. Del Genio (2010), Black carbon semi-direct effects on cloud cover: Review and synthesis, *Atmos. Chem. Phys.*, *10*, 7685–7696, doi:10.5194/acp-10-7685-2010.

Koren, I., Y. J. Kaufman, D. Rosenfeld, L. A. Remer, and Y. Rudich (2005), Aerosol invigoration and restructuring of Atlantic convective clouds, *Geophys. Res. Lett*, *32*, L14828, doi:10.1029/2005GL023187.

Koren, I., J. V. Martins, L. A. Remer, and H. Afargan (2008), Smoke invigoration versus inhibition of clouds over the Amazon, *Science*, *321*, 946.

Lerach, D. G., and W. R. Cotton (2011), Comparing aerosol and low-level moisture influences on supercell tornadogenesis: Three-dimensional idealized simulations, *J. Atmos. Sci.*, *69*, 969–987, doi:10.1175/jas-d-11-043.1.

Lerach, D. G., B. J. Gaudet, and W. R. Cotton (2008), Idealized simulations of aerosol influences on tornadogenesis, *Geophys. Res. Lett.*, *35*, L23806, doi:10.1029/2008GL035617.

Li, Z., F. Niu, J. Fan, Y. Liu, D. Rosenfeld, and Y. Ding (2011), Long-term impacts of aerosols on the vertical development of clouds and precipitation, *Nat. Geosci.*, *4*, 888–894. [Available at http://www.nature.com/ngeo/journal/v4/n12/abs/ngeo1313.html#supplementary-information.]

Lyons, W. A., T. E. Nelson, E. R. Williams, J. A. Cramer, and T. R. Turner (1998), Enhanced positive cloud-to-ground lightning in thunderstorms ingesting smoke from fires, *Science*, *282*, 77–80, doi:10.1126/science.282.5386.77.

Markowski, P. M., and Y. P. Richardson (2009), Tornadogenesis: Our current understanding, forecasting considerations, and questions to guide future research, *Atmos. Res.*, *93*, 3–10, doi:10.1016/j.atmosres.2008.09.015.

Markowski, P. M., J. M. Straka, and E. N. Rasmussen (2002), Direct surface thermodynamic observations within the rear-flank downdrafts of nontornadic and tornadic supercells, *Mon. Weather Rev.*, *130*, 1692–1721, doi:10.1175/1520-0493(2002)130<1692:dstowt>2.0.co;2.

Markowski, P., C. Hannon, J. Frame, E. Lancaster, A. Pietrycha, R. Edwards, and R. L. Thompson (2003), Characteristics of vertical wind profiles near supercells obtained from the Rapid Update Cycle, *Weather Forecasting*, *18*, 1262–1272, doi:10.1175/1520-0434(2003)018<1262:covwpn>2.0.co;2.

McFiggans, G., P. Artaxo, U. Baltensperger, H. Coe, M. Facchini, G. Feingold, S. Fuzzi, M. Gysel, A. Laaksonen, and U. Lohmann (2006), The effect of physical and chemical aerosol properties on warm cloud droplet activation, *Atmos. Chem. Phys.*, *6*, 2593–2649.

Morcrette, J. J., et al. (2009), Aerosol analysis and forecast in the European Centre for Medium-Range Weather Forecasts Integrated Forecast System: Forward modeling, *J. Geophys. Res.*, *114*, D06206, doi:10.1029/2008JD011235.

Morrison, H., G. Thompson, and V. Tatarskii (2009), Impact of cloud microphysics on the development of trailing stratiform precipitation in a simulated squall line: Comparison of one- and two-moment schemes, *Mon. Weather Rev.*, *137*, 991–1007, doi;10.1175/2008mwr2556.1.

Mulcahy, J. P., D. N. Walters, N. Bellouin, and S. F. Milton (2014), Impacts of increasing the aerosol complexity in the Met Office global numerical weather prediction model, *Atmos. Chem. Phys.*, *14*, 4749–4778, doi:10.5194/acp-14-4749-2014.

Murray, N. D., R. E. Orville, and G. R. Huffines (2000), Effect of pollution from central American fires on cloud-to-ground lightning in May 1998, *Geophys. Res. Lett.*, *27*, 2249–2252, doi:10.1029/2000GL011656.

NOAA (2011), The historic tornadoes of April 2011, National Oceanic and Atmospheric Administration Service Assessment. [Available at http://www.nws.noaa.gov/om/assessments/index.shtml.]

©2015. American Geophysical Union. All Rights Reserved.

Rasmussen, E. N., and D. O. Blanchard (1998), A baseline climatology of sounding-derived supercell and tornado forecast parameters, *Weather Forecasting*, *13*, 1148–1164, doi:10.1175/1520-0434(1998)013<1148:abcosd>2.0.co;2.

Rosenfeld, D. (2000), Suppression of rain and snow by urban and industrial air pollution, *Science*, *287*, 1793–1796, doi:10.1126/science.287.5459.1793.

Rosenfeld, D., and T. L. Bell (2011), Why do tornados and hailstorms rest on weekends?, *J. Geophys. Res.*, *116*, D20211, doi:10.1029/2011JD016214.

Rosenfeld, D., and T. L. Bell (2013), Reply to comment by S. E. Yuter et al. on "Why do tornados and hailstorms rest on weekends?", *J. Geophys. Res. Atmos.*, *118*, 7339–7343, doi:10.1002/jgrd.50539.

Rosenfeld, D., U. Lohmann, G. B. Raga, C. D. O'Dowd, M. Kulmala, S. Fuzzi, A. Reissell, and M. O. Andreae (2008), Flood or drought: How do aerosols affect precipitation?, *Science*, *321*, 1309–1313, doi:10.1126/science.1160606.

Rosenfeld, D., M. Clavner, and R. Nirel (2011), Pollution and dust aerosols modulating tropical cyclones intensities, *Atmos. Res.*, *102*, 66–76, doi:10.1016/j.atmosres.2011.06.006.

Saide, P. E., G. R. Carmichael, Z. Liu, C. S. Schwartz, H. C. Lin, A. M. da Silva, and E. Hyer (2013), Aerosol optical depth assimilation for a size-resolved sectional model: Impacts of observationally constrained, multi-wavelength and fine mode retrievals on regional scale analyses and forecasts, *Atmos. Chem. Phys.*, *13*, 10,425–10,444, doi:10.5194/acp-13-10425-2013.

Schuster, G. L., O. Dubovik, and B. N. Holben (2006), Angstrom exponent and bimodal aerosol size distributions, *J. Geophys. Res.*, *111*, D07207, doi:10.1029/2005JD006328.

Stensrud, D. J., et al. (2009), Convective-scale warn-on-forecast system, *Bull. Am. Meteorol. Soc.*, *90*, 1487–1499, doi:10.1175/2009bams2795.1.

Thompson, G., and T. Eidhammer (2014), A study of aerosol impacts on clouds and precipitation development in a large winter cyclone, *J. Atmos. Sci.*, *71*, 3636–3658, doi:10.1175/jas-d-13-0305.1.

Thompson, R. L., R. Edwards, J. A. Hart, K. L. Elmore, and P. Markowski (2003), Close proximity soundings within supercell environments obtained from the Rapid Update Cycle, *Weather Forecasting*, *18*, 1243–1261, doi:10.1175/1520-0434(2003)018<1243:cpswse>2.0.co;2.

Thompson, R. L., B. T. Smith, J. S. Grams, A. R. Dean, and C. Broyles (2012), Convective modes for significant severe thunderstorms in the contiguous United States. Part II: Supercell and QLCS tornado environments, *Weather Forecasting*, *27*, 1136–1154, doi:10.1175/waf-d-11-00116.1.

Twomey, S. (1991), Aerosols, clouds and radiation, *Atmos. Environ. Part A*, *25*, 2435–2442.

Wang, J., S. van den Heever, and J. Reid (2009), A conceptual model for the link between central American biomass burning aerosols and severe weather over the south central United States, *Environ. Res. Lett.*, *4*, 015003, doi:10.1088/1748-9326/4/1/015003.

Wilcox, E. M. (2010), Stratocumulus cloud thickening beneath layers of absorbing smoke aerosol, *Atmos. Chem. Phys.*, *10*, 11,769–11,777, doi:10.5194/acp-10-11769-2010.

Xue, H., G. Feingold, and B. Stevens (2008), Aerosol effects on clouds, precipitation, and the organization of shallow cumulus convection, *J. Atmos. Sci.*, *65*, 392–406, doi:10.1175/2007jas2428.1.

Yuan, T., L. A. Remer, and H. Yu (2011), Microphysical, macrophysical and radiative signatures of volcanic aerosols in trade wind cumulus observed by the A-Train, *Atmos. Chem. Phys.*, *11*, 7119–7132, doi:10.5194/acp-11-7119-2011.

Yuter, S. E., M. A. Miller, M. D. Parker, P. M. Markowski, Y. Richardson, H. Brooks, and J. M. Straka (2013), Comment on "Why do tornados and hailstorms rest on weekends?" by D. Rosenfeld and T. Bell, *J. Geophys. Res. Atmos.*, *118*, 7332–7338, doi:10.1002/jgrd.50526.

Zaveri, R. A., and L. K. Peters (1999), A new lumped structure photochemical mechanism for large-scale applications, *J. Geophys. Res.*, *104*, 30,387–30,415, doi:10.1029/1999JD900876.

Zaveri, R. A., R. C. Easter, J. D. Fast, and L. K. Peters (2008), Model for simulating aerosol interactions and chemistry (MOSAIC), *J. Geophys. Res.*, *113*, D13204, doi:10.1029/2007JD008782.

Ziegler, C. L., E. R. Mansell, J. M. Straka, D. R. MacGorman, and D. W. Burgess (2010), The impact of spatial variations of low-level stability on the life cycle of a simulated supercell storm, *Mon. Weather Rev.*, *138*, 1738–1766, doi:10.1175/2009mwr3010.1.

©2015. American Geophysical Union. All Rights Reserved.